THE JOURNAL OF BIOLOGICAL CHEMISTRY
Vol. 273, No. 43, Issue of October 23, pp. 28199–28207, 1998
Printed in U.S.A.

Crystal Structure of the Catalytic Domain of Protein-tyrosine Phosphatase SHP-1*

(Received for publication, July 10, 1998)

Jian Yang‡, Xiaoshan Liang‡, Tianqi Niu‡, Wuyi Meng‡§, Zhizhuang Zhao¶, and G. Wayne Zhou‡‖

From the ‡Program in Molecular Medicine, University of Massachusetts Medical Center, Worcester, Massachusetts 01605 and ¶Department of Medicine, Vanderbilt University, Nashville, Tennessee 37232

The crystal structures of the protein-tyrosine phosphatase SHP-1 catalytic domain and the complex it forms with the substrate analogue tungstate have been determined and refined to crystallographic *R* values of 0.209 at 2.5 Å resolution and 0.207 at 2.8 Å resolution, respectively. Despite low sequence similarity, the catalytic domain of SHP-1 shows high similarity in secondary and tertiary structures with other protein-tyrosine phosphatases (PTPs). In contrast to the conformational changes observed in the crystal structures of PTP1B and *Yersinia* PTP, the WPD loop (Trp^{419}-Pro^{428}) in the catalytic domain of SHP-1 moves away from the substrate binding pocket after binding the tungstate ion. Sequence alignment and structural analysis suggest that the residues in the WPD loop, especially the amino acid following Asp^{421}, are critical for the movement of WPD loop on binding substrates and the specific activity of protein-tyrosine phosphatases. Our mutagenesis and kinetic measurements have supported this hypothesis.

Protein-tyrosine phosphatases (PTPs)[1] are a family of enzymes that catalyze the dephosphorylation of phosphotyrosine peptides. PTPs, together with the protein-tyrosine kinases, regulate the critical phosphotyrosine levels in the signal transduction pathways. PTPs can be divided into two groups: receptor-like PTPs and cytosolic PTPs. The receptor-like PTPs have highly conserved tandem intracellular catalytic domains and a diversity of receptor-like extracellular domains implicated in cell signaling. The cytosolic PTPs, however, contain a single conserved catalytic domain linked to a variety of noncatalytic segments that presumably exert a regulatory and/or targeting function. Among these noncatalytic segments are Src homology 2 (SH2) domains, which are found in SHPs, an extensively studied subfamily of intracellular PTPs. SHPs consist of SHP-1 (also called PTP1C, SH-PTP1, HCP, SHP, and PTPN6), SHP-2 (also called PTP2C, SH-PTP2, PTP1D, SH-PTP3, and Syp) and Csw from *Drosophila* (1–3). They contain two SH2 domains followed by a catalytic domain and an inhibitory C terminus. In biological systems, SHPs can be viewed as enzymes that exist primarily in the inactive state within resting cells. The inhibition of the activity of SHPs was attributable to the insertion of a D′-E loop (Asn^{58}-Tyr^{62}) of the N-terminal SH2 domain into the substrate binding pocket (4). After cell stimulation, SHPs would translocate from cytosol to plasma membrane and bind to the tyrosine-phosphorylated receptors through their SH2 domains, becoming activated in the process. Although they belong to the same family and have similar catalytic and regulatory mechanisms, SHP-1 and SHP-2 have different biological functions *in vivo*.

SHP-1 is highly expressed in hematopoietic cells. It has been identified as the gene responsible for causing the *me* and me^v mouse phenotypes (5, 6), which cause profound abnormalities in the immune system. In addition, SHP-1 is one of the most extensively studied PTPs, functioning in hematopoietic cells as a terminator of signaling transduction predominantly by dephosphorylation of appropriate substrates (7–10). In contrast, SHP-2 is expressed in most cell types. It is involved in the signal transduction stimulated by epidermal growth factor, platelet-derived growth factor, and insulin. After stimulation, SHP-2 is phosphorylated at its C-terminal end. The phosphorylated SHP-2 has been shown to bind Grb2 with its C-terminal end and to bind receptors such as epidermal growth factor receptor, platelet-derived growth factor receptor, and insulin receptor substrate -1 *via* its SH2 domains. Grb2 behaves as an adapter molecule that links mSOS to SHP-2. This complex then activates *ras* and the mitogen-activated protein kinase pathway. Therefore, SHP-2 serves as a positive regulator of cell proliferation (11–14).

The crystal structures of the catalytic domains of different PTPs, including PTP1B (15, 16), *Yersinia* PTP (17), PTPα (18), PTPμ (19), and SHP-2 (4), have been determined using protein crystallography. Structural and kinetic analyses have identified two important amino acids, Cys^{215} in the PTP signature motif and Asp^{181} in the WPD loop (PTP1B numbering), as the primary active site residues that attack substrates. Here we report the crystal structures of the catalytic domain of protein-tyrosine phosphatase SHP-1 and of the complex it forms with tungstate, the substrate analogue. The structural comparison of SHP-1 with other protein-tyrosine phosphatases has revealed an additional amino acid that contributes to the activity of tyrosine phosphatase.

EXPERIMENTAL PROCEDURES

Crystallization and Data Collection—Detailed procedures for expression, purification, crystallization, and data collection have been reported (20). The catalytic domain of human SHP-1 (amino acids 245–543) was cloned and expressed into an *Escherichia coli* expression system and purified by ion exchange and affinity chromatography. Crystals were obtained from reservoir solution containing 15% polyethylene glycol 10,000, 0.1 M Hepes, pH 7.5. A 2.5-Å diffraction data set was reprocessed with the programs DENZO and SCALEPACK (21). The space group is $P2_1$, with new cell dimensions of a = 41.82 Å, b =

* This work was supported by a Career Development Award from the American Diabetes Association and other support from the Melheim Foundation, American Cancer Society, Massachusetts Division, and National Research on Leukemia Association, Inc. The costs of publication of this article were defrayed in part by the payment of page charges. This article must therefore be hereby marked "*advertisement*" in accordance with 18 U.S.C. Section 1734 solely to indicate this fact.

§ Present address: Laboratory of Molecular Medicine, Harvard Medical School, Boston, MA 02115.

‖ To whom correspondence should be addressed: Program in Molecular Medicine, University of Massachusetts Medical Center, 373 Plantation St., Worcester, MA 01605. Tel.: 508-856-6869; Fax: 508-856-4289; E-mail: zhou@ummed.edu.

[1] The abbreviations used are: PTP, protein-tyrosine phosphatase; SH2, Src homology 2; p-NPP, *p*-nitrophenol phosphate; ES, enzyme substrate; r.m.s., root mean square.

87.78 Å, c = 43.00 Å, and β = 117.4°. There is one molecule per asymmetric unit. The final R_{sym} of the diffraction data is 8.2%, and the data completeness is 99.7% up to 2.5-Å resolution.

Crystals of the catalytic domain of SHP-1 complexed with tungstate were obtained by soaking the native catalytic domain crystals in the cryosolvent (50% polyethylene glycol 10,000, 0.1 M Hepes, pH 7.5, 15% glycerol) containing 5 mM tungstate for up to 24 h. A 2.8-Å resolution data set was collected at −188 °C, using an ADSC cryosystem and MAR imaging plate (Area Detector Systems Corp., CA) with the x-ray source generated from a Rigaku (Japan) RU-300 operating at 50 kV and 100 mA. The complex data was also processed by DENZO and SCALEPACK (21). The unit cell of the tungstate complex is a = 42.21 Å, b = 87.48 Å, c = 44.21 Å, and β = 120.1°. The R_{sym} of the diffraction data is 8.7% with completeness of 94.7% up to 2.8-Å resolution.

Structure Determination and Refinement—The molecular replacement method was used to solve the phase problem of the catalytic domain of SHP-1. The crystal structure of PTP1B (Protein Data Bank code 2HNP), with the deleted side chains of the nonconserved amino acids and the deleted loop regions, which are different between the overlapped PTP1B and *Yersinia* PTP structures, was used as the search model. A molecular replacement solution was found using the program AMoRe (22). The solution was refined by rigid body and positioning using X-PLOR (23). The electron density map was calculated with X-PLOR and displayed on Silicon Graphics workstations using TURBO-FRODO (24). The missing side chains were added to the model. The model was then refined for 23 cycles using the slow-cool and positional refinement protocols in the X-PLOR package using the data between 6 and 2.5 Å ($F > 2\sigma F$). The free R value (25) was also calculated from the first to the penultimate cycle by randomly selecting 5% of the data as the test set. The free R in the penultimate cycle was 29.3%. In the last cycle, all 7392 reflections in the range of 6–2.5 Å were used in the refinement, and the final crystallographic R value was 20.9%. There were 2736 non-hydrogen atoms in the final model. No solvent molecules were added. The r.m.s. deviations of bond distances and bond angles from ideal geometry were 0.014 Å and 2.1°, respectively. The tungstate ion position in the complex structure was located directly from the difference electron density map contoured at 3.5σ level. This complex structure was refined to a crystallographic R value of 20.7% and a free R factor of 28.7%, using the data between 6 and 2.8 Å. The r.m.s. deviations of bond distances and bond angles for the complex structure were 0.014 Å and 1.9°, respectively.

Mutagenesis and Kinetic Measurements—The H422Q and H422F mutants were cloned into pT7 vector by standard polymerase chain reaction cloning techniques using two primers corresponding to both strands of the mutation site and two primers previously used for cloning the catalytic domain of SHP-1 (20). These mutants were expressed and purified using the same procedure as used for wild-type proteins. The kinetic measurements were performed at room temperature and pH 5.0 using published protocols (26). The total reaction volume was 100 μl, containing both PTPs and substrate in the working buffer (50 mM NaOAc-HOAc, pH 5.0, 2 mM EDTA, 2 mM dithiothreitol, 40% glycerol). For substrate *p*-nitrophenol phosphate (*p*-NPP), the reaction was quenched by adding 900 μl of 0.2 M NaOH. Concentration of the released product, *p*-nitrophenol, was measured by A_{410} with an extinction coefficient of 17.8/mM. For the activity assay against substrate phosphotyrosine, the malachite green method (27) was used to measure the release of inorganic phosphate. At first, the standard A_{660} *versus* [$PO_4^{=}$] curve was measured as the standard for the determination of the released phosphate concentration. The reaction procedure was the same as used for *p*-NPP, except that malachite green mix (3 volume of 0.045% malachite green hydrochloride in water and 1 volume of 4.2% ammonium molybdate in 4 M HCl) was used to quench the reaction. The kinetic parameters were defined from double reciprocal plots.

RESULTS

Secondary and Tertiary Structure of the Catalytic Domain of SHP-1—The crystal structure of the catalytic domain of SHP-1 was determined by a molecular replacement method, using the coordinates of PTP1B as the search model. The tungstate ion position in the complex structure was identified directly from the difference electron density map contoured at 3.5σ level. The structures of the catalytic domain and the complex it forms with tungstate have been refined to final crystallographic R values of 0.209 at 2.5 Å resolution and 0.207 at 2.8 Å resolution, respectively. The electron density map around the active site of SHP-1 is shown in Fig. 1*a*. The catalytic domain of SHP-1 contains residues 245–543 of SHP-1, the SH2-containing protein-tyrosine phosphatase cloned from a human breast carcinoma cDNA library (28). However, the model of the catalytic domain comprises only residues 250–532. The N-terminal 5 residues and the C-terminal 11 residues were not observed in the electron density map. Residues Leu^{402} and Asp^{403}, which are located on a surface loop, are also absent in the model. Summary of data collection and refinement statistics are listed in Table I. The geometry of the final models of both the native enzyme and the complex was examined with the program PROCHECK (29). The native enzyme structure had all of the residues in the allowed regions of the Ramachandran plot, and the complex structure had 99.6% of the residues in the allowed regions of the Ramachandran plot.

The structure of the catalytic domain of SHP-1 (Fig. 1*b*) can be divided into a core region and the extended N and C termini. Both termini interact with the crystallographic symmetry-related molecules. The N terminus points toward the substrate binding site of a symmetry-related molecule. The catalytic domain of SHP-1 is an α/β protein containing 12 β strands and 6 α helices. A highly twisted β sheet, formed by 10 β strands, spans the entire core region. The center region of the sheet is formed by four parallel β strands, β3, β12, β4, and β11. The twisted β sheet has also been observed in other PTPs structures (4, 15–19, 30). The other two β strands, β5 and β6, which form a β-loop-β motif, are involved in substrate binding. In addition, four α helices, which form a four-helix bundle, were flanked over one side of the twisted sheet, and the remaining two were located on the other side. Differing from the PTP1B structure, the catalytic domain of SHP-1 has several insertions and deletions. These insertions and deletions occur on the surface loops. Although the catalytic domain of SHP-1 bears low sequence identity (38%) with the catalytic domain of PTP1B, its three-dimensional structure closely resembles that of PTP1B. The r.m.s. difference between the Cα atoms of the catalytic domain of SHP-1 and those of PTP1B is only 0.8 Å. The sequence alignments of the catalytic domain of SHP-1 with the catalytic domains of other PTPs are shown in Fig. 2. The PTP signature motif HC*X*AG*X*GR(S/T) is highly conserved in the catalytic domains of PTPs.

Active Site and Substrate Binding Pocket of SHP-1—The binding site for phosphotyrosine is a deep pocket on the surface of the protein. The active site, formed by the PTP signature motif HC*X*AG*X*GR(S/T), is located at the bottom of the phosphotyrosine binding pocket (Fig. 1*b*). The four sides of the binding pocket are formed by the β5-loop-β6 motif, part of helix α1 with the loop between helix α1 and strand β1, the loop between helices α5 and α6, and the WPD loop (Trp^{419}-Pro^{428}) between strand β11 and helix α3. Electrostatic potential calculation shows that the bottom of the phosphotyrosine binding pocket has large positive electrostatic potentials (Fig. 3*f*). In addition, a few protrusions and depressions are clearly observed on the surface of the molecule around the phosphotyrosine binding pocket. Compared with the phosphotyrosine binding pocket, those potential binding subsets are relatively shallow and open to the solvent. After superimposing the structure of the catalytic domain of SHP-1 with the structure of PTP1B-hexapeptide complex (16), four basic residues (Lys^{273}, Lys^{279}, Arg^{277}, and Arg^{360}) that could potentially interact with the phophotyrosine peptide substrates were identified at the minus end of the SHP-1 phosphotyrosine binding pocket. The surface electrostatic potential calculation (Fig. 3*f*) also shows that the minus end of the phosphotyrosine binding pocket has positive electrostatic potentials. Those results suggest that SHP-1 prefers substrates with acidic residues N-terminal to the phosphotyrosine residue.

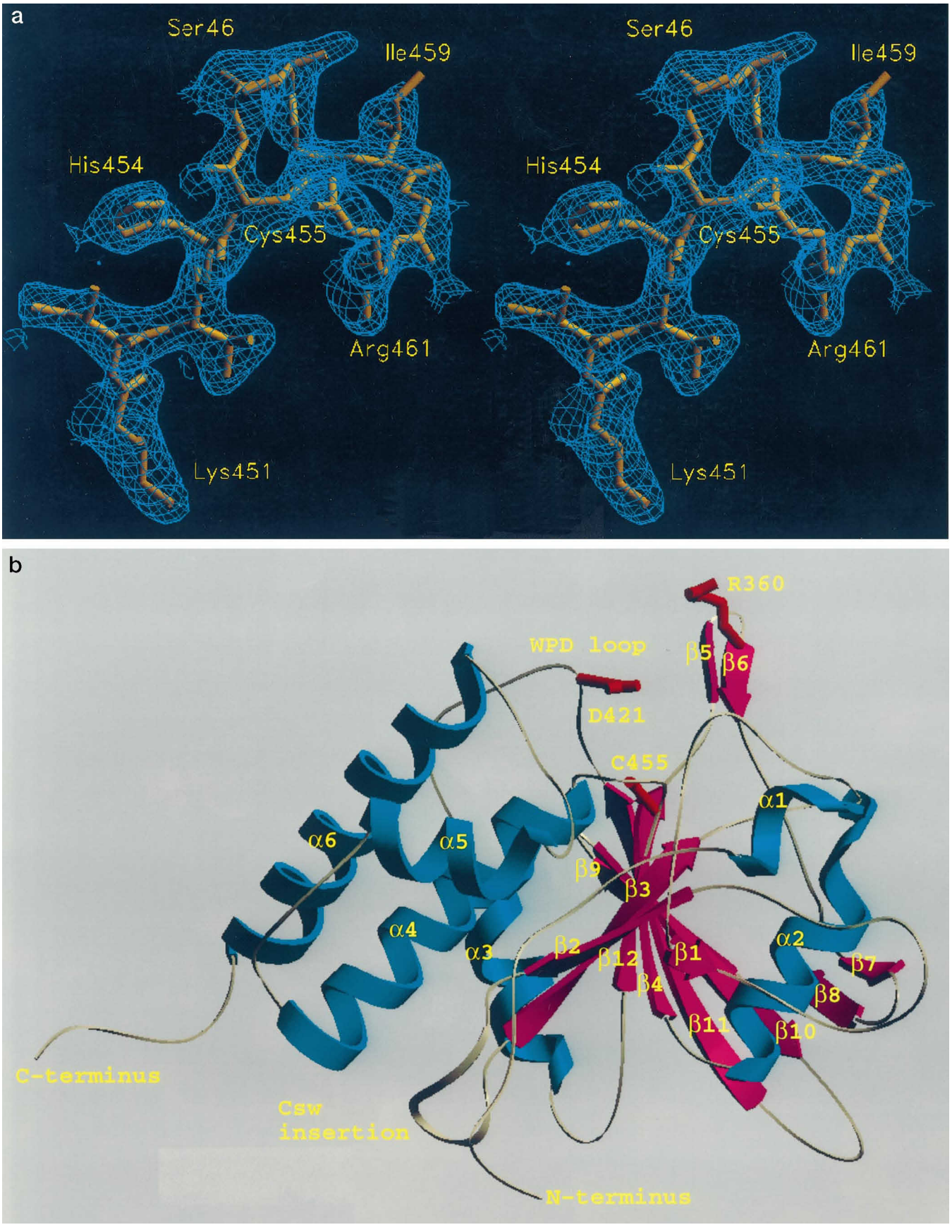

FIG. 1. **The electron density map ($2F_o - F_c$) at the active site (*a*) and a ribbon representation of the catalytic domain of SHP-1, showing the secondary structure and the overall folding (*b*).** β sheets are *pink*; α helices are *blue*. Side chains of the active site residues Cys^{455} and Asp^{421} are shown in *red*. Residue Arg^{360} identified the mutation sites for insertion and deletion in the *me*^{v} mice. The 155-residue insertion region in Csw is also labeled. This figure was prepared by SETOR (38).

TABLE I
Crystal data and refinement results

	SHP-1	SHP-1/WO_4
Crystal data		
Unit cell	a = 41.82Å; b = 87.78Å; c = 43.00Å; β = 117.4°	a = 42.21Å; b = 87.48Å; c = 44.21Å; β = 120.1°
Space group	$P2_1$	$P2_1$
Resolution (Å)	2.5	2.8
Data collecting temperature (°C)	−188	−188
R_{merge} (%)	8.2	8.7
Data completeness (%)	99.7	94.7
Number of unique reflections	8779	6544
Refinement		
R value	20.9	20.7
R free	29.3	28.7
Resolution range (Å)	6–2.5	6–2.8
Number of reflections used in refinement	7392	5426
Total number of non-H atoms	2736	2755
Estimate coordinate error (Å)	0.3	0.3
R.m.s. differences for bond distances (Å)	0.014	0.014
R.m.s. differences for bond angles (°)	2.1	1.9
R.m.s. differences for dihedral angles (°)	28.4	28.1
R.m.s. differences for impropers (°)	0.9	0.9

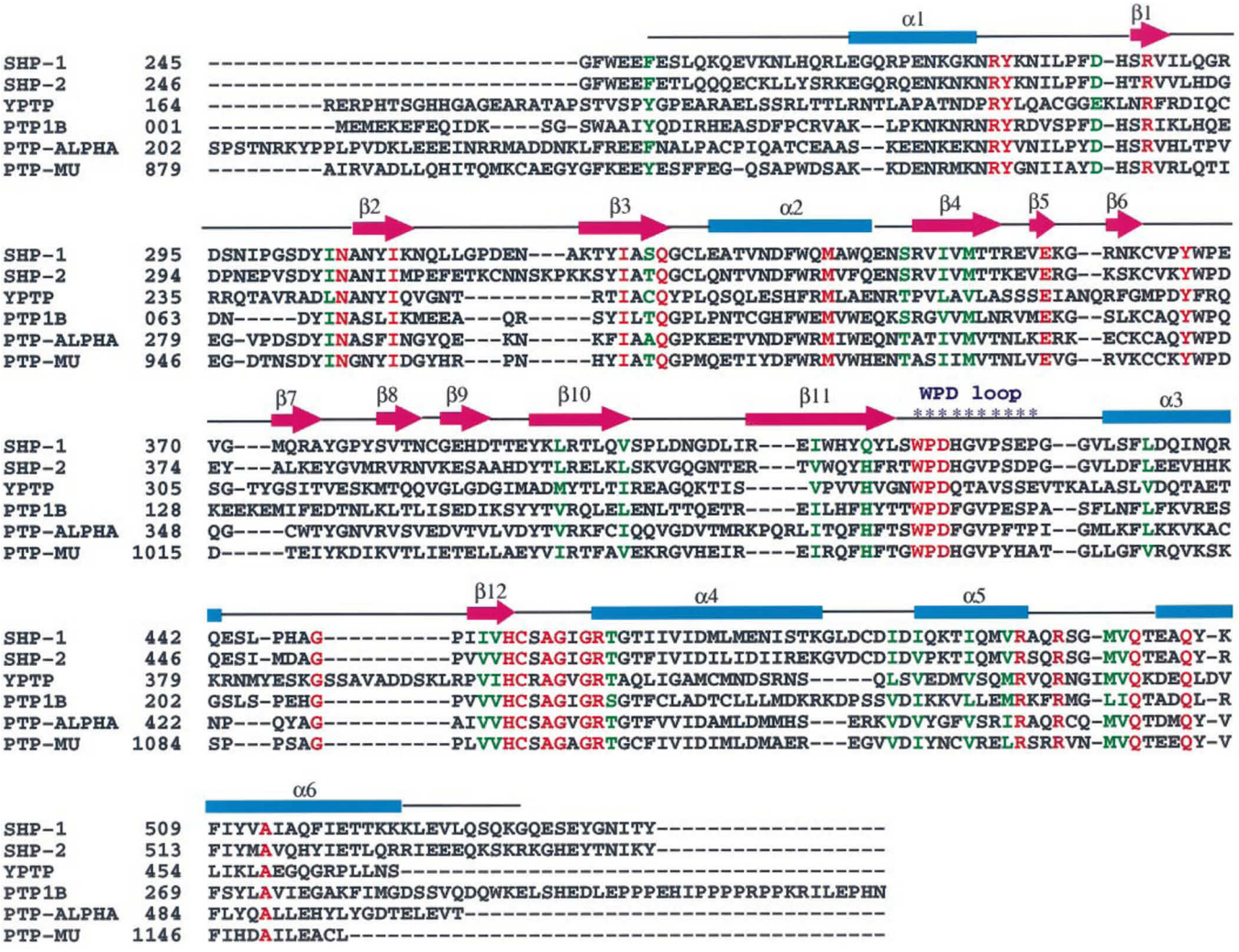

FIG. 2. **Sequence alignments of the catalytic domains of SHP-1 with the catalytic domains of SHP-2, *Yersinia* PTP, PTP1B, PTPα, and PTPμ.** The identical residues are shown in *red*, and the homology residues are shown in *green*. The secondary structures of the catalytic domain of SHP-1 are also shown.

The active site Cys^{455} is located in the PTP signature motif, which is a loop between strand β12 and helix α4. Previous studies have shown that the active site cysteine residue in PTPs is present as a thiolate anion at physiological pH (31) and acts as a nucleophile in the dephosphorylation reaction (15). Compared with its position in the native structure, the side chain of Cys^{455} shifted 0.5–1.0 Å toward the tungstate ion in the SHP-1-tungstate complex structure. Three weak hydrogen bonds are formed between the O1, O2, and O3 atoms of the tungstate ion and the sulfur atom of Cys^{455}. In addition, nine

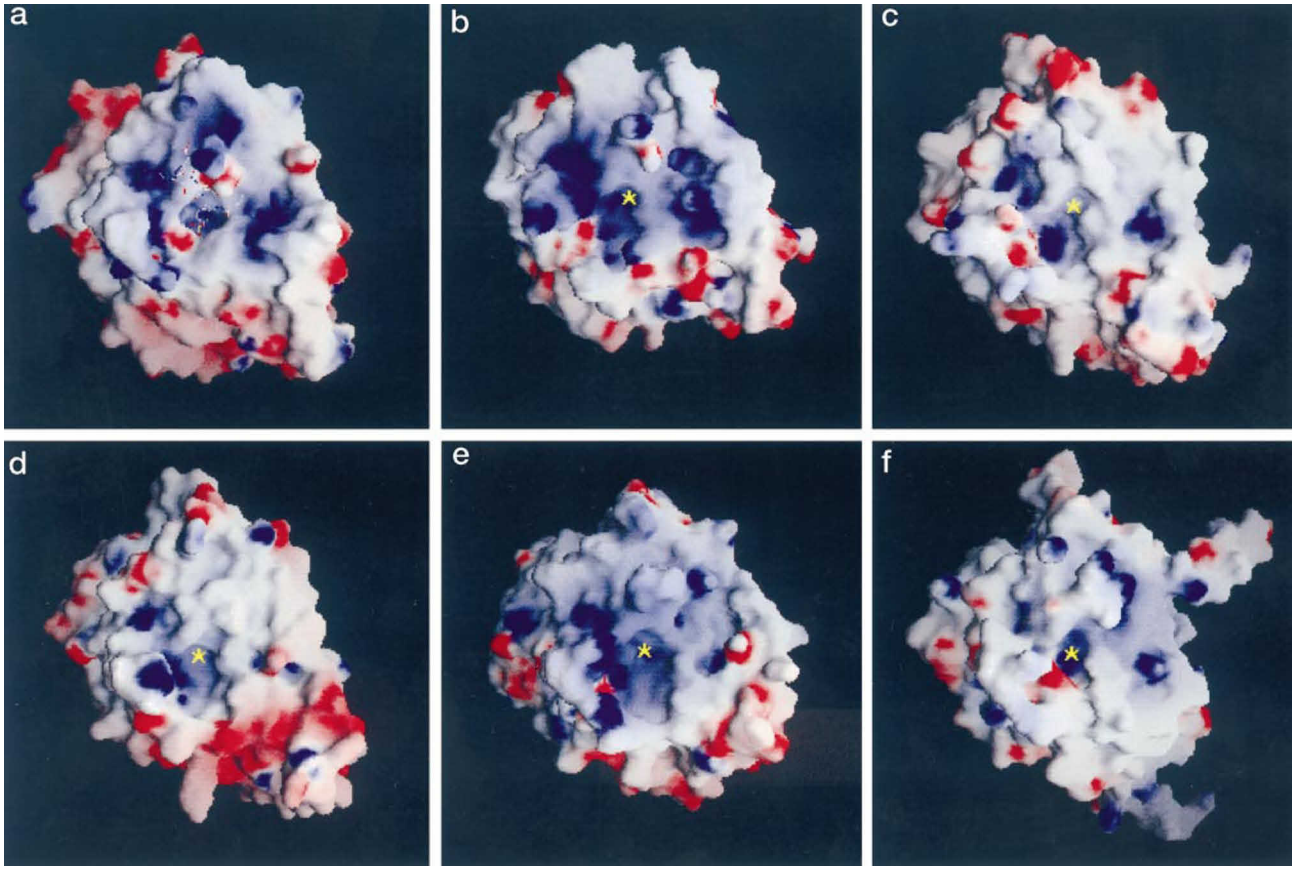

FIG. 3. **Surface electrostatic potentials of the catalytic domains of PTP1B (*a*), *Yersinia* PTP (*b*), PTPα (*c*), PTPμ (*d*), SHP-2 (*e*), and SHP-1 (*f*).** *Red* and *blue* represent negative and positive electrostatic potentials, respectively. This figure was prepared by GRASP (39).

hydrogen bonds are formed between SHP-1 and the tungstate; eight are formed between the signature motif and the tungstate ion. Fig. 4 is a diagram of the hydrogen bonds between the catalytic domain of SHP-1 and tungstate.

Biological Relevance of the Crystal Structure—Mutations in SHP-1 have been found to be the molecular cause of the phenotypes of moth-eaten (*me*) and moth-eaten viable (me^v) mice, which have profound autoimmunity and immune deficiency consequent to a severe disruption of hemopoietic cell development and function (32). In me^v mice, two mutations (me^v/me^v 1000 and me^v/me^v 1100) were identified in the catalytic domain region with a 5-residue deletion and a 23-residue insertion at the Arg^{360} site located in the β5-loop-β6 motif (Fig. 1*b*). Because this region forms part of the phosphotyrosine binding pocket, the deletion mutation would shorten the substrate binding pocket, whereas the insertion mutation would result in an extended loop, which might fold back and block the substrate binding pocket. These mutants, therefore, would decrease the dephosphorylation activity of SHP-1 and dysfunction of the hemopoietic cell development pathway. On the other hand, Csw, the SH2-containing protein-tyrosine phosphatase in *Drosophila*, has a 155-residue insertion (3) in the loop region between strands β2 and β3 (Fig. 1*b*). Because this insertion is far from the catalytic site, it may not cause interference with substrate binding. However, this large insertion could form another domain, which might interact with other proteins in signal transduction pathways.

Comparison with Other PTP Structures—Comparing the catalytic domain of SHP-1 with other PTP structures has identified a novel conformational change of the WPD loop after substrate binding. In Fig. 5, we show the overlapping structures of different forms (the native form and the tungstate or phosphotyrosine binding form) of *Yersinia* PTP, PTP1B, and the catalytic domain of SHP-1. The PTPs are shown in *yellow* in the native structure, in *red* in the complexes with tungstate, and in *dark red* in the PTP1B-hexapeptide complex. The active site cysteine is located at the *bottom* of each figure. In *Yersinia* PTP, the major structural change observed after tungstate binding is the movement of the WPD loop toward the active site (from *yellow* to *red*). However, no conformational change was observed in the WPD loop region after binding tungstate in PTP1B (*yellow* and *red*). The WPD loop moves toward the active site after binding the hexapeptide substrate (from *yellow* and *dark red*). Whereas in the SHP-1 structure, the WPD loop moves away from the active site (*yellow* to *red*) after binding the substrate analogue tungstate.

The WPD loop was previously identified as part of the phosphotyrosine binding pocket (16). Residue Asp^{181}, located at the tip of WPD loop of PTP1B (equivalent to Asp^{421} in SHP-1 and Asp^{356} in *Yersinia* PTP), is the critical residue involved in the dephosphorylation reaction. It acts as a hydrogen donor to release the tyrosine peptide in the first step of the reaction. It then activates a water molecule to hydrolyze the thiophosphate intermediate in the second step of the reaction. Therefore, the translocation of the WPD loop after binding the substrate (Fig. 5, *a* and *b*) will move the aspartic acid toward the active site and locate it close to the substrate.

Because of the importance of the aspartate residue in the dephosphorylation reaction, its accurate position in the active site after the substrate binding is crucial to the dephosphorylation activity. The position of this aspartic acid in the active site is achieved by the translocation of the WPD loop and is stabilized by the interactions between the WPD loop and the substrate. In the *Yersinia* PTP structure (17), tungstate binding moves the WPD loop 3.3 Å toward the active site so that Asp^{356} and Gln^{357} can form two hydrogen bonds with the tung-

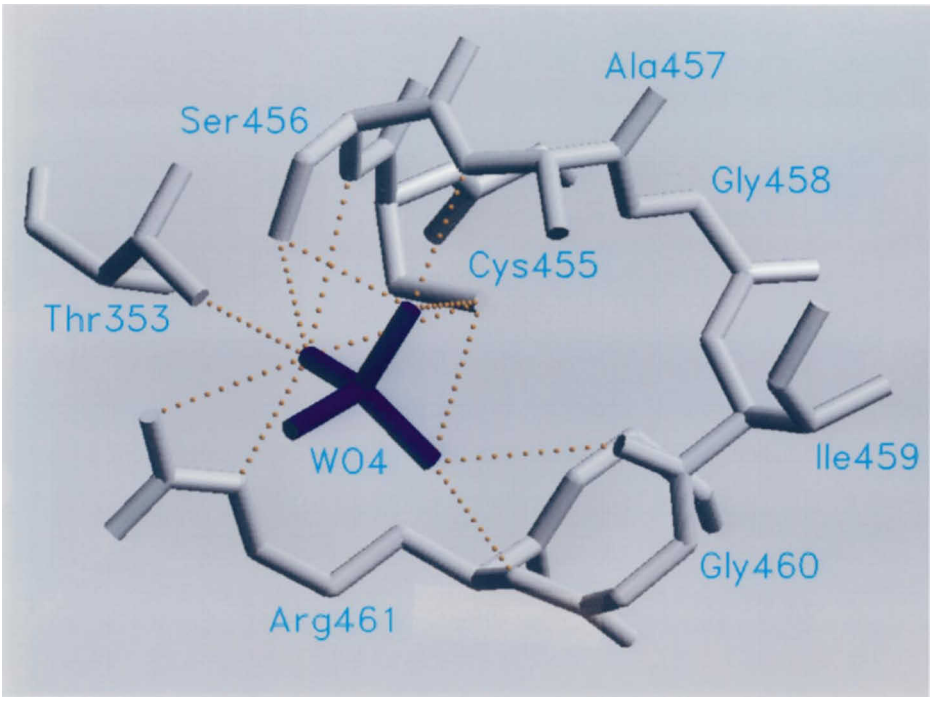

FIG. 4. **Representation showing the hydrogen bonds formed between the catalytic domain of SHP-1 and the substrate analogue tungstate ion.**

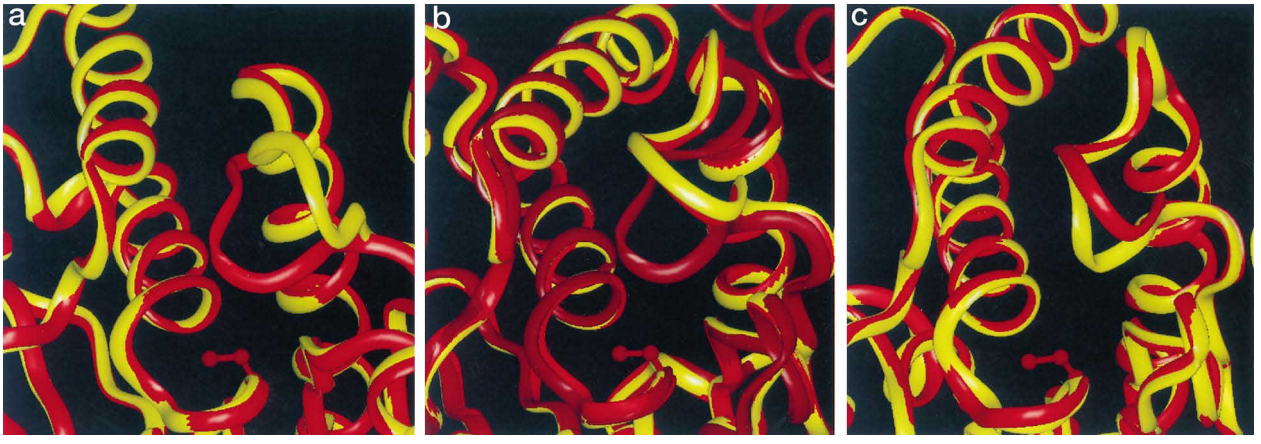

FIG. 5. **Comparison of the WPD loop movements in *Yersinia* PTP (*a*), PTP1B (*b*), and the catalytic domain of SHP-1 (*c*) after binding tungstate ion (all 3 enzymes) or phosphotyrosine peptides (PTP1B).** The native enzyme structures are shown in *yellow*; the tungstate complex structures are shown in *red*; and the phosphotyrosine peptide-PTP1B complex structure is shown in *dark red*. This figure was prepared by InsightII (Molecular Simulations Inc., San Diego, CA).

state ion *via* the $O_{\delta 1}$ and $N_{\epsilon 2}$ atoms, respectively. The amino acid equivalent to Gln^{357} in *Yersinia* PTP is Phe^{182} in PTP1B, which cannot interact with tungstate in the PTP1B-tungstate complex. Therefore, no conformational change was observed in the structure of the WPD loop region of PTP1B after binding tungstate. However, in the PTP1B-hexapeptide complex, the WPD loop moves ~3.5 Å toward the active site (16). This active WPD loop conformation is stabilized by the hydrogen bond between Asp^{181} and the phosphate group of the phosphotyrosine and by the π-π interactions between Phe^{182} and the phenyl ring of the phosphotyrosine. In the SHP-1 structure, the amino acid equivalent to Gln^{357} is His^{422}. Because the side chain of His^{422} is one carbon group shorter than the side chain of Gln, it is too short to form hydrogen bonds with the tungstate and to stabilize the active WPD loop conformation. Besides, unidentified repulsion forces push the WPD loop away from the active site after tungstate binding (Fig. 5*c*). Therefore, the movement of WPD loop after substrate binding is very possibly correlated with the amino acid after the critical aspartic acid residue in the WPD loop.

Detailed comparison of the WPD loop in native SHP-1 structure shows that it differs from other native PTP structures. For the convenience of discussion, we refer to the WPD conformation in the native PTP1B structure as the "open, inactive" conformation (Fig. 5*b*, *yellow*) and the WPD conformation in the PTP1B-hexapeptide complex structure as the "closed, active" conformation (Fig. 5*b*, *dark red*). Overlapping SHP-1 with PTP1B shows that the WPD loop in the SHP-1 tungstate complex is in the open conformation. However, the WPD loop in the SHP-1 native structure is in a half-open, half-closed conformation. Asp^{421} is in the conformation similar to those of Asp^{181} and Asp^{356} in the PTP1B-hexapeptide and *Yersinia* PTP-tungstate complex structures, respectively, whereas His^{422} is in the conformation similar to those of Phe^{182} and Gln^{357} in the PTP1B native and *Yersinia* PTP native structures. Comparing the backbone of the WPD loop region in the native SHP-1 structure (Fig. 5*c*, *yellow*) with the backbones of the WPD loops in PTP1B native and PTP1B-hexapeptide complex structures (Fig. 5*b*, *yellow* and *dark red*) also shows the half-open, half-closed conformation. The electron density maps around the WPD loop region are shown in Fig. 6 for both the native SHP-1 structure and the tungstate complex.

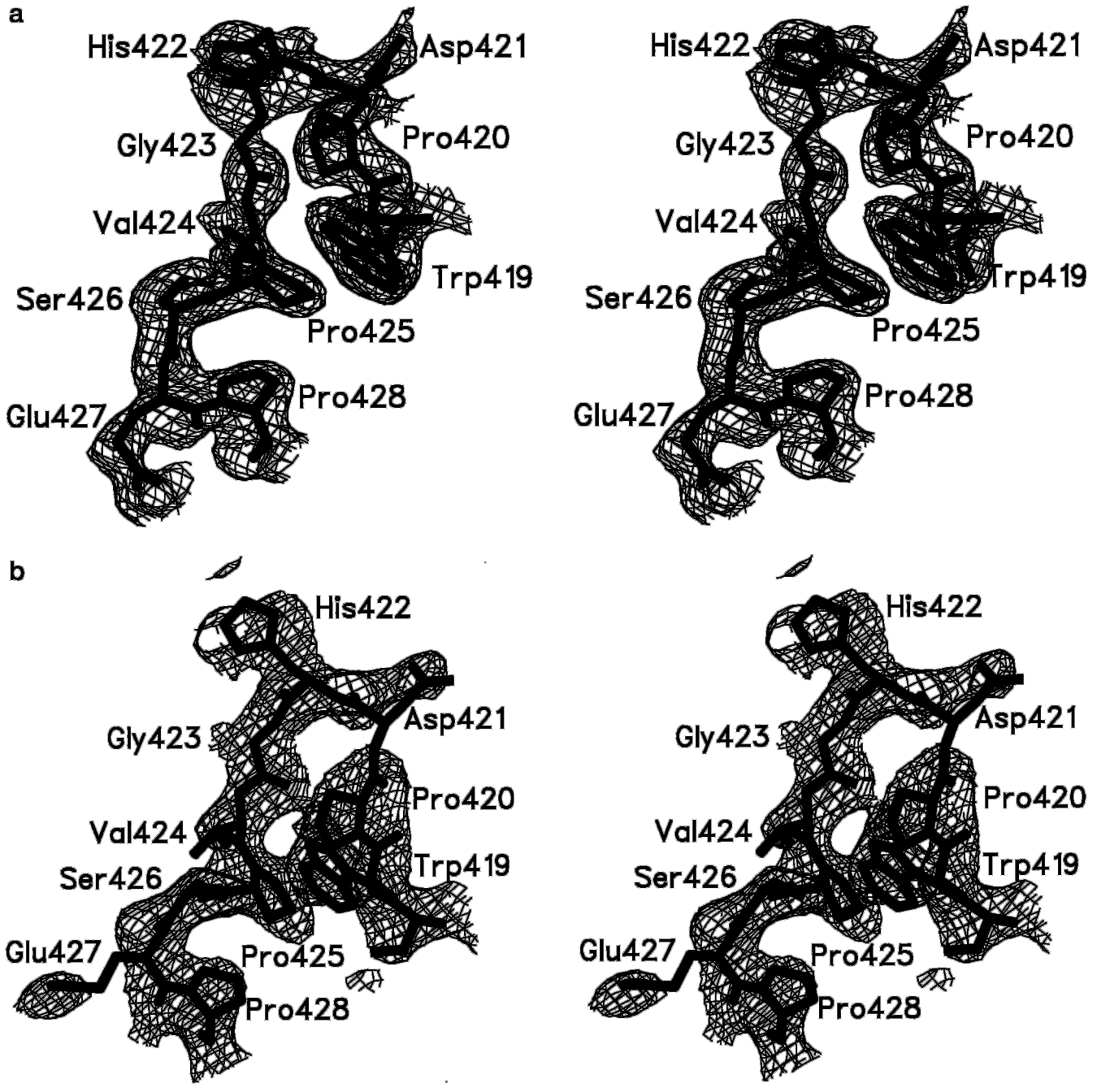

FIG. 6. **The electron density maps ($2F_o - F_c$) at the WPD loop region in both the native (*a*) and the complex (*b*) structures.** The contour level is 1σ. This figure was prepared by SETOR (38).

The different movements of the WPD loop after substrate binding for different PTPs may be caused by crystallization condition or crystal packing. To check the effects of crystallization, we examined the crystallization conditions of the catalytic domain of SHP-1, PTP1B, SHP-2, and *Yersinia* PTP. Crystals of all PTPs were grown with polyethelene glycol as the precipitant at very similar pH values (7.0–7.5) (4, 15–17, 33). All tungstate complexes were obtained by soaking the native crystals in precipitant solutions or cryosolvents containing the tungstate ion. In addition, we have examined the effects of crystal packing. The WPD loop does not interact with symmetry-related molecules and is not involved in crystal packing. Therefore, the conformational change of the WPD loop among different PTPs should be related to different PTPs.

Comparison of the Catalytic Domains of SHP-1 and SHP-2—The special location of Asp^{421} in the SHP-1 native structure was further supported by comparing it with the full-length SHP-2 structure. While we were preparing the manuscript, the crystal structure of full-length SHP-2, another member in the SH2 domain-containing protein-tyrosine phosphatase family, was determined by x-ray crystallography (4). Although the sequence identity between the catalytic domains of SHP-1 and SHP-2 is only ~60%, the superimposed Cα atoms of the catalytic domains of SHP-1 and SHP-2 share extremely high similarity in both the secondary and tertiary structures, with the r.m.s. deviation of 0.6 Å. The most obvious difference between the catalytic domains of SHP-1 and SHP-2 is that both N and C termini in the structure of the catalytic domain of SHP-1 are extended away from the molecule. This may be partly attributable to crystal packing in SHP-1, where both termini are interacting with the symmetry-related molecules.

Another major difference between these two structures is the

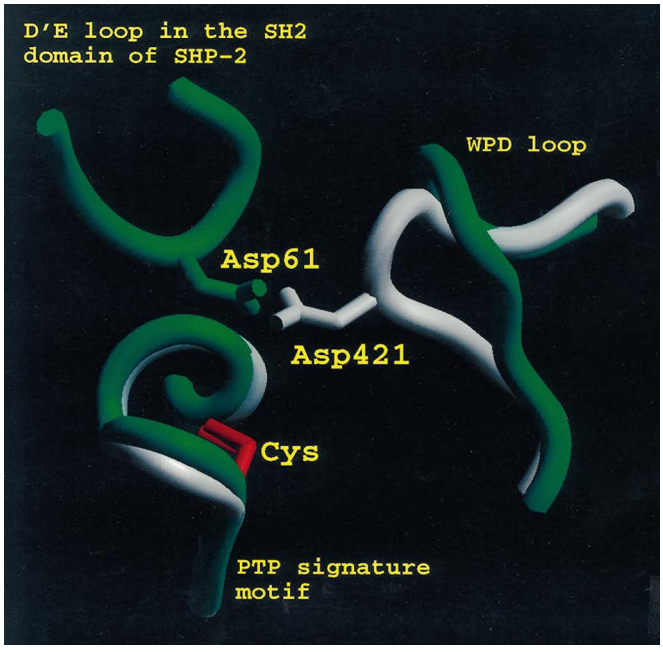

FIG. 7. **Substrate binding pocket of the catalytic domain of SHP-1 after superimposition with SHP-2, showing that Asp^{421} in SHP-1 occupies a similar place as Asp^{61} does in SHP-2.** SHP-1 and SHP-2 are shown in *white* and *green*, respectively.

WPD loop. In the SHP-2 structure, the WPD loop is close to the position of the WPD loop in the SHP-1-tungstate complex structure in the open, inactive conformation. In addition, the inhibition of the full-length SHP-2, as identified from the SHP-2 structure, was attributable to the intrusion of D′-E loop (Asn^{58}-Tyr^{62}) from the N-terminal SH2 domain into the phosphotyrosine binding pocket of the catalytic domain of SHP-2. Although the binding of the D′-E loop into the phosphotyrosine binding pocket mimics some features of substrate binding, the bulky D′-E turn may prevent the WPD loop from forming the closed, active conformation (4). Unexpectedly, the side chain of Asp^{421} in the catalytic domain of SHP-1 occupies a place similar to the place occupied by Asp^{61} in the D′-E loop of SHP-2 (Fig. 7). Therefore, one possible explanation is that there might be a "trap" for the negatively charged residue around the aspartic residue binding site of SHPs. This trap attracts Asp^{61}, stabilizes the N-terminal SH2 domain in the inhibiting position, and pushes the WPD loop into the open conformation (as found in the SHP-2 structure). After removing the SH2 domain (as determined in the SHP-1 structure), the trap can attract Asp^{421} in the SHP-1 structure and locate it in the closed conformation. The rest of the WPD loop, however, remains in the open conformation, because there are no other interactions to stabilize the WPD loop in the closed conformation. Therefore, the WPD loop is located in a half-open, half-closed form, as determined from the crystal structure of SHP-1. After binding the tungstate, the repulsion force between Asp^{421} and tungstate will push Asp^{421} away from the active site and locate the WPD loop in the open conformation. Occupation of the similar site by two different aspartic acid residues supports the trap hypothesis. However, no direct interactions within 3.5 Å were observed between Asp^{61} and other amino acids in the crystal structure of SHP-2 and between Asp^{421} and other amino acids in SHP-1. Residues Thr^{59}, Tyr^{62}, Thr^{69}, Lys^{366}, Ser^{460}, and Arg^{465} were within 5 Å of the carboxyl group of Asp^{61} in SHP-2. Residues Thr^{59}, Tyr^{62}, and Thr^{69} were from the N-terminal SH2 domain. In SHP-1, residues Glu^{357}, Ser^{456}, Arg^{461}, and Gln^{506} were within 5 Å of the carboxyl group of Asp^{421} and were the potential residues contributing to the anion trap.

TABLE II
Summary of the kinetic parameters (k_{cat} and K_m)

	p-NPP		pY	
	k_{cat}	K_m	k_{cat}	K_m
	s^{-1}	mM	s^{-1}	mM
Yersinia PTP	1234[a]	2.4[a]	164[b]	9.6[b]
PTP1B	75.3[c]	0.89[c]	72.9[c]	2.01[c]
Catalytic domain of SHP-1	125.8	1.26	59.8	0.44
Catalytic domain of SHP-1 (H422F)	173.1	1.85	ND[d]	>5
Catalytic domain of SHP-1 (H422Q)	295.5	3.10	90.1	0.91

[a] Ref. 36.
[b] Ref. 37.
[c] Ref. 33.
[d] ND, cannot be determined because the curve is still in the linear range.

Previous studies on swapping the catalytic domains of SHP-1 and SHP-2 have suggested that both SHP-1 and SHP-2 have different specific substrates (34, 35). To get a peer view of the substrate specificities, we calculated the surface electrostatic potentials of both SHP-1 and SHP-2 and compared them with other PTPs (Fig. 3). At the minus end of the phosphotyrosine binding pocket, the electrostatic potentials are much more positive in SHP-2 than in SHP-1. Large positive electrostatic potentials are also observed on the plus side of the phosphotyrosine binding pocket in SHP-2. The different electrostatic distribution at the potential substrate binding pocket, therefore, supports that SHP-1 and SHP-2 have different substrate specificities.

DISCUSSION

The significant discovery made by studying the structure of the catalytic domain of SHP-1 is the novel WPD loop movement after substrate binding. The different WPD loop movements for different PTPs after substrate binding have been correlated with the interactions between the WPD loop and the binding substrate. The movement of the WPD loop is probably dependent on the amino acid after the critical aspartic acid residue in the WPD loop. Because of the interactions between Gln^{357} and the tungstate in *Yersinia* PTP, the WPD loop was stabilized in the closed conformation after tungstate binding. In PTP1B, the corresponding amino acid is Phe^{182}, which cannot interact with tungstate but can interact with the phenyl ring of the tyrosine side chain. Therefore, WPD loop movement was only observed after phosphotyrosine binding. In SHP-1, however, the corresponding amino acid of Gln^{357} in *Yersinia* PTP is His^{422}, the side chain of which is one carbon shorter than Gln. Therefore, the WPD loop is still located in the open position after tungstate binding. We cannot predict what conformation the WPD loop will be in the co-crystal structure of SHP-1 with phosphotyrosine peptides.

The WPD loop of the catalytic domain of SHP-1 in the native structure was in a half-open, half-closed conformation. Aspartic acid Asp^{421} occupied the position that was occupied by Asp^{61} in the N-terminal SH2 domain of SHP-2. This half-open, half-closed conformation should block and decrease the substrate binding of SHP-1, because Asp^{421} should be in the open position before any substrate could enter into the substrate binding pocket.

The above structural comparisons suggest that the WPD loop is stabilized in the closed, active conformation in the following order (from easy to difficult): *Yersinia* PTP, PTP1B, and SHP-1. SHP-1 needs to change from the half-open conformation to the open conformation before it can bind the substrate. If we assume that the easier (less energy) it is to move the WPD loop into the active conformation, the more active the PTP will be, then the order for the PTP activity should be, from high to low, *Yersinia* PTP, PTP1B, and SHP-1. Using phosphotyrosine as

the substrate, the k_{cat} values for the catalytic domains of *Yersinia* PTP, PTP1B, and SHP-1 are 164 s^{-1} (36), 72.9 s^{-1} (37), and 59.8 s^{-1}, respectively, consistent with the prediction.

As an approximation, the K_m can be considered as $(k_{-1} + k_2)/k_1$. Therefore, if an enzyme has a decreased reaction rate k_2 (namely, reduced ES $\rightarrow$ E + P reaction), the enzyme substrate complex [ES] would increase in concentration. This increase would then accelerate the dissociation of the [ES] complex (namely increase reaction rate k_{-1} for ES $\rightarrow$ E + S reaction) and decrease the formation of the ES complex (namely, decrease k_1, the reaction rate for the E + S $\rightarrow$ ES reaction). Because k_2 is usually much less than k_1, K_m is mainly determined by k_{-1}/k_1. As explained above, decreased product release rate k_2 would increase k_{-1} and decrease k_1, resulting in an increase of the K_m. As shown in the PTP1B-hexapeptide complex structure, Phe^{182} forms hydrophobic interactions with the tyrosine ring. Compared with SHP-1, those interactions would stabilize the product of the reaction, the tyrosine residue and, therefore, would prevent the product release. Therefore, PTP1B would have a higher K_m than SHP-1. In fact, K_m for PTP1B (2.01 mM) is higher than K_m for the catalytic domain of SHP-1 (0.44 mM) when using phosphotyrosine peptide as the substrate.

One prediction made from structural analysis of SHP-1 is that the a Gln replacement of His^{422} in the catalytic domain of SHP-1 should increase the activity k_{cat} but have little effect on K_m, whereas mutating His^{422} to Phe should increase the apparent binding constant K_m. To examine these predictions, we prepared two mutants, H422Q and H422F. We have measured the dephosphorylation activity of these proteins *versus* the artificial substrates *p*-NPP and phosphotyrosine (Table II). As predicted, k_{cat} of the H422Q mutant increased 2- to 3-fold using *p*-NPP as the substrate and 50% using phosphotyrosine as the substrate. Because SHP-1 is an enzyme that has been chosen by evolution, a 3-fold increase on its activity by a single mutation is an significant change. In addition, the H422F mutant exhibits increased K_m, from 1.26 to 1.85 mM using *p*-NPP as the substrate and from 0.44 to $>$ 5 mM using phosphotyrosine as the substrate. Therefore, both structural and mutation studies indicate that the WPD loop plays an important role in the determination of the specific activity of different PTPs.

To establish the biological significance of the above results, we have aligned 356 different PTP sequences around the WPD loop region. Based on the amino acid types at positions 421 and 422 (SHP-1 numbering system), the sequences can be divided into three general categories: DH, DF(DY), and DQ. Among the 356 WPD loop sequences, 175 sequences have DH, 62 sequences have either DF or DY, and 5 sequences have DQ at these two positions in the WPD loop. We also found that 34 PTPs have EQ at these two positions in the WPD loop.

Protein-tyrosine phosphatases are generally considered terminators for cell growth-signaling pathways. Because of their lower k_{cat} and low K_m values, we propose that the catalytic domain of the DH-type phosphatases respond and terminate signals at low phosphotyrosine levels. Such phosphatases generally have high substrate specificity. For example, swapping the catalytic domains of SHP-1 and SHP-2 cannot replace their negative biological functions (34, 35). In contrast, when the phosphotyrosine concentration *in vivo* is too high, the catalytic domain of DF-type phosphatases may be important for signal termination. These phosphatases generally have high activity. The DQ-type phosphatases from bacteria such as *Yersinia* may have special functions, such as the disruption of the signal transduction system of host cells. These phosphatases generally have high dephosphorylation activity and low substrate specificity. Therefore, DH, DF, and DQ are proposed as three major types of protein-tyrosine phosphatases. SHP-1, PTP1B, and *Yersinia* PTP are representatives of these three categories.

Acknowledgments—We thank Drs. Roger Davis, Michael Czech, and Michael Green for critical reading of the manuscript. We are also in debt to Drs. Steven E. Shoelson and Michael J. Eck (Harvard Medical School) for providing the coordinates of the full-length SHP-2.

REFERENCES

1. Neel, B. G. (1993) *Semin. Cell Biol.* **4,** 419–432
2. Feng, G. S., and Pawson, T. (1994) *Trends Genet.* **10,** 54–58
3. Neel, B. G., and Tonks, N. K. (1997) *Curr. Opin. Cell Biol.* **9,** 193–204
4. Hof, P., Pluskey, S., Dhe-Paganon, S., Eck, M. J., and Shoelson, S. E. (1998) *Cell* **92,** 441–450
5. Shultz, L. D., Schweitzer, P. A., Rajan, T. V., Yi, T., Ihle, J. N., Matthews, R. J., Thomas, M. L., and Beier, D. R. (1993) *Cell* **73,** 1445–1454
6. Tsui, H. W., Siminovitch, K. A., de Souza, L., and Tsui, F. W. (1993) *Nat. Genet.* **4,** 124–129
7. Klingmüller, U., Lorentz, U., Cantley, L. C., Neel, B. G., and Lodish, H. F. (1995) *Cell* **80,** 729–738
8. D'Ambrosio, D., Hippen, K. L., Minskoff, S. A., Mellman, I., Pani, G., Siminovitch, K. A., and Cambier, J. C. (1995) *Science* **268,** 293–297
9. Plas, D. R., Johnson, R., Pingel, J. T., Matthews, R. J., Dalton, M., Roy, G., Chan, A. C., and Thomas, M. L. (1996) *Science* **272,** 1173–1176
10. Ono, M., Okada, H., Bolland, S., Yanagi, S., Kurosaki, T., and Ravetch, J. V. (1997) *Cell* **90,** 293–301
11. Bennett, A. M., Tang, T. L., Sugimoto, S., Walsh, C. T., and Neel, B. G. (1994) *Proc. Natl. Acad. Sci. U. S. A.* **91,** 7335–7339
12. Xiao, S., Rose, D. W., Sasaoka, T., Maegawa, H., Burke, T. R., Jr., Roller, P. P., Shoelson, S. E., and Olefsky, J. M. (1994) *J. Biol. Chem.* **269,** 21244–21248
13. Noguchi, T., Matozaki, T., Horita, K., Fujioka, Y., and Kasuga, M. (1994) *Mol. Cell. Biol.* **14,** 6674–6682
14. Yamauchi, K., Milarski, K. L., Saltiel, A. R., and Pessin, J. E. (1995) *Proc. Natl. Acad. Sci. U. S. A.* **92,** 664–668
15. Barford, D., Flint, A. J., and Tonks, N. K. (1994) *Science* **263,** 1397–1404
16. Jia, Z., Barford, D., Flint, A. J., and Tonks, N. K. (1995) *Science* **268,** 1754–1758
17. Stuckey, J. A., Schubert, H. L., Fauman, E. B., Zhang, Z. Y., Dixon, J. E., and Saper, M. A. (1994) *Nature* **370,** 571–575
18. Bilwes, A. M., den Hertog, J., Hunter, T., and Noel, J. P. (1996) *Nature* **382,** 555–559
19. Hoffmann, K. M., Tonks, N. K., and Barford, D. (1997) *J. Biol. Chem.* **272,** 27505–27508
20. Liang, X., Meng, W., Niu, T., Zhao, Z., and Zhou, G. W. (1997) *J. Struct. Biol.* **120,** 201–203
21. Otwinowski, Z., and Minor, W. (1997) *Methods Enzymol.* **276,** 307–326
22. Navaza, J. (1994) *Acta Crystallogr. Sect. A* **50,** 157–163
23. Brünger, A. T. (1992) *X-PLOR Manual Version 3.1.* Yale University, New Haven, CT
24. Roussel, A., Foutecilla-Camps, J. C., and Cambillau, C. (1990) *Acta Crystallog. Sect. A* **46,** C66
25. Brünger, A. T. (1992) *Nature* **55,** 472–475
26. Zhao, Z., Bouchard, P., Diltz, C. D., Shen, S. H., and Fischer, E. H. (1993) *J. Biol. Chem.* **268,** 2816–2820
27. Harder, K. W., Owen, P., Wong, L. K. H., Aebersold, R., Clark-Lewis, I., and Jirik, F. R. (1994) *Biochem. J.* **298,** 395–401
28. Shen, S. H., Bastien, L., Posner, B. I., and Chrétien, P. (1991) *Nature* **352,** 736–739
29. Laskowski, R. A., MacArthur, M. W., Hutchinson, S. G., and Thornton, J. M. (1993) *J. Appl. Crystallogr.* **26,** 283–291
30. Su, X. D., Taddei, N., Stefani, M., Ramponi, G., and Nordlund, P. (1994) *Nature* **370,** 575–578
31. Zhang, Z. Y., and Dixon, J. E. (1993) *Biochemistry* **32,** 9340–9345
32. Bignon, J. S., and Siminovitch, K. A. (1994) *Clin. Immunol. Immunopathol.* **73,** 168–179
33. Zhang, Z. Y., Clemens, J. C., Schubert, H. L., Stuckey, J. A., Fischer, M. W. F., Hume, D. M., Saper, M. A., and Dixon, J. E. (1992) *J. Biol. Chem.* **267,** 23759–23766
34. Tenev, T., Keilhack, H., Tomic, S., Stoyanov, B., Stein-Gerlach, M., Lammers, R., Krivtsov, A. V., Ullrich, A., and Böhmer, F. D. (1997) *J. Biol. Chem.* **272,** 5966–5973
35. O'Reilly, A. M., and Neel, B. G. (1998) *Mol. Cell. Biol.* **18,** 161–177
36. Zhang, Z. Y., Maclean, D., McNamara, D. J., Sawyer, T. K., and Dixon, J. E. (1994) *Biochemistry* **33,** 2285–2290
37. Zhang, Z. Y. (1995) *J. Biol. Chem.* **270,** 11199–11204
38. Evans, S. V. (1993) *J. Mol. Graph.* **11,** 134–138
39. Nicholls, A., Sharp, K., and Honig, B. (1991) *Proteins Struct. Funct. Genet.* **11,** 281–296